Analysis of Torque Production in Axial-flux Vernier PM Machines of the MAGNUS Type

Murat G. Kesgin
SPARK Lab., ECE Dept.
University of Kentucky
Lexington KY, USA
murat.kesgin@uky.edu

Peng Han
ANSYS, Inc
San Jose, CA, USA
peng.han@ieee.org

Damien Lawhorn
SPARK Lab., ECE Dept.
University of Kentucky
Lexington KY, USA
damien.lawhorn@uky.edu

Dan M. Ionel
SPARK Lab., ECE Dept.
University of Kentucky
Lexington KY, USA
dan.ionel@ieee.org

***Abstract*—The paper presents a study of the torque production in a novel vernier-type axial-flux permanent magnet (PM) machine topology named MAGNUS. Two computational methods are employed, one based on the 3D FEA Maxwell stress calculations on individual stator and rotor components and one based on the analytical derivation of the air-gap flux density harmonics. Examples are provided for a design with a 40-pole spoke-type PM rotor and two stators, one active including a 3-phase winding with 6 concentrated coils wound around main teeth in a single layer arrangement and a second stator that has neither coils nor main slots and is profiled towards the airgap in the same way as the active stator. It is shown that auxiliary small teeth included in the stator main teeth yield a significant increase in the output torque and that the profiled stator has a lower contribution than the active stator to the total torque. A brief report on the ongoing development of a prototype motor is included.**

***Index Terms*—Vernier-type, high-torque, axial-flux permanent magnet machine, MAGNUS**

I. Introduction

Permanent magnet (PM) synchronous machines with high specific torque have been a major subject of ongoing research, e.g. [1], [2].. Among different topologies, machines of the vernier-type in axial-flux (AF) configurations have been reported to have great potential in this respect and were considered as suitable candidates for direct-drive low-speed applications, such as in-wheel traction and wind turbine generators. Important advantages of vernier-type motors include a very low number of stator coils, which may simplify the manufacturing of stator windings, combined with high rotor polarities that provide opportunities for magnetic flux concentration [3]–[5].

This paper continues on previously published work from the authors' extended research group on a proposed vernier-type configuration introduced under the name of MAGNUS [4]. The feasible slot-pole combinations for 2-phase and 3-phase versions have been established and the 2-phase arrangement has been studied in [6]. A large-scale optimization study based on three-dimensional (3-D) finite element analysis (FEA) for a MAGNUS AF machine with two special stators and one spoke-type PM rotor was previously published [7].

Further contributions to the subject matter are brought in this paper by studying the torque production and its components with examples from a 3-phase MAGNUS machine, which has 40 rotor poles but only 6 coils wound on the main stator teeth in a single layer arrangement (Fig.1(a)). The stator winding is advantageous in terms of simplified manufacturing, as well as improved tolerance, because phase coils are placed in separate slots [8]. In the active stator, which includes the winding, each main stator tooth has 2 auxiliary teeth. The second stator has neither coils nor main slots and is profiled towards the air-gap in the same way as the active stator. The two stators are rotated relatively to each other by one rotor pole pitch, in order to minimize flux leakage and increase the torque output and the power factor. The rotor is of the spoke PM type, which yields high flux concentration and specific magnetic loading.

The 3-D FEA provides accurate prediction based on detailed geometry modeling and having a large number of elements, requiring substantial time and powerful computing systems. In [9], analytical equations of torque, back electromotive force (EMF), cogging torque and power factor have been derived based on the vernier-type motor geometry. Analytical derivations and 2D-FEA for dual-stator vernier-type axial-flux machine have been studied in [10]. Analysis of electromagnetic performance based on air gap flux density harmonics has been proposed for switched-flux permanent-magnet in-stator [11]. The torque production mechanism of the studied MAGNUS machine has not been discussed thoroughly. The current paper examines the torque contributions in the MAGNUS machine following the torque decomposition approaches based on air-gap flux density waveforms, aiming at gaining insights into the torque production of such machines and establishing its design rules.

The paper is organized as follows. In section II, torque contributions of stator and rotor components based FEA analysis are presented. In section III, a harmonic-based torque decomposition method in the studied topology is introduced. PM field and torque analytical developments are discussed in section IV. Prototyping of a MAGNUS motor and its corresponding test fixture are introduced in section V. Section

[*]Dr. Peng Han was with the SPARK Laboratory, ECE Department, University of Kentucky, Lexington, KY and is now with ANSYS Inc., San Jose, CA, USA

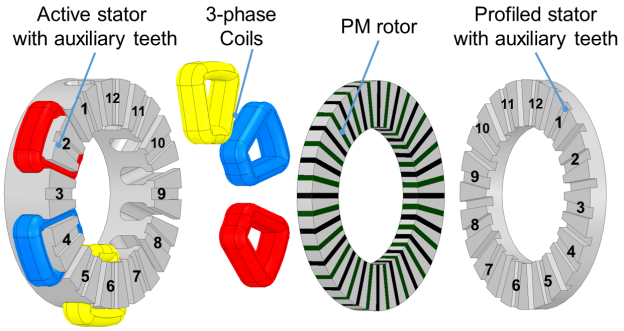

(a)

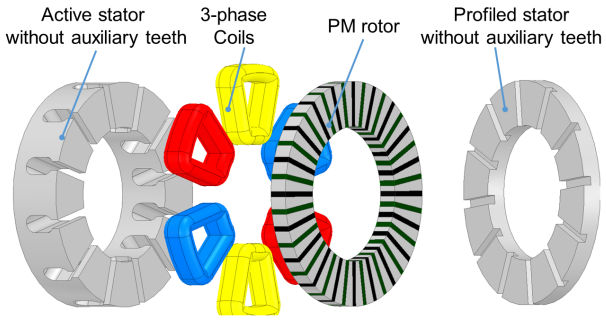

(b)

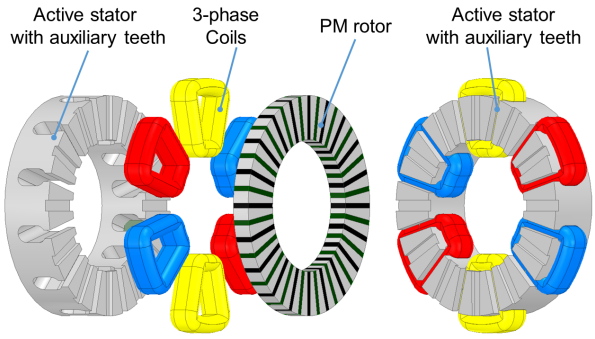

(c)

Fig. 1: Exploded view of proposed topology versions of vernier-type AFPM machine of the MAGNUS type (a) one wound stator and one profiled stator, (b) one wound stator and one profiled stator but no auxiliary teeth, (c) two wound stators.

VI concludes the paper and discusses the further work.

II. Torque Contribution by Rotor and Stators

The torque contribution of each stator and rotor components has been examined by integrating the tangential component of the Maxwell Stress Tensor over the component surfaces using:

$$f_t(t,\theta) = \frac{B_a(t,\theta)B_t(t,\theta)}{\mu_o} \tag{1}$$

where $B_a(t,\theta)$ and $B_t(t,\theta)$ are the axial and tangential flux densities calculated by FEA. The tangential force on the individual stator teeth and rotor components can be evaluated

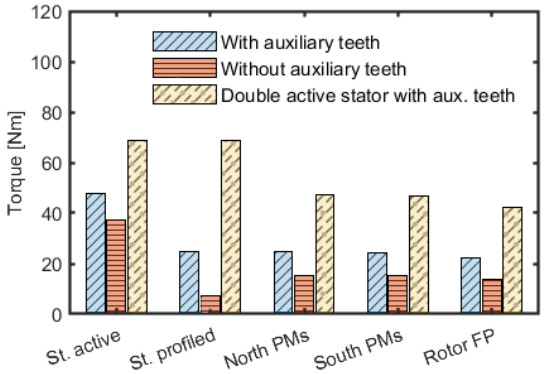

Fig. 2: Torque breakdown in motor components for the studied three topologies.

by integrating the stress over the corresponding mechanical components as follows:

$$F_t = \int_S f_t(t,\theta)\,dS. \tag{2}$$

Torque breakdown for the studied MAGNUS machine calculated from this approach is illustrated in Fig. 2 and shows that the active stator produces almost twice the torque than the profiled stator without winding. In the rotor, the average torque is almost equally distributed over the rotor components. The torque generated by each PM and rotor ferromagnetic pole (FP) is 1.2 Nm and 0.6 Nm, respectively. The sum of the torque by all rotor components is 71.0 Nm.

Contributions of the stator teeth are listed in Table I. The teeth surrounded by coils are numbered with even numbers and are the main contributors to torque production. The profiled stator tooth labeled by odd numbers only generate a low and negative torque. Most flux lines are passing through stator teeth labeled by even numbers as shown in Fig. 3.

Two other topologies shown in Fig. 1(b) and Fig. 1(c) have also been modeled. Their torque breakdowns are also illustrated in a way similar to the studied MAGNUS machine in Fig. 2. It is shown that auxiliary teeth increase the torque production by introducing additional torque-contributing harmonics and reduce flux leakage. Torque waveforms of the models are demonstrated in Fig. 4, showing relatively low torque ripple.

TABLE I: Individual torque contribution by each stator tooth.The teeth labeled even number contribute higher torque than odd number.

Components	Torque [Nm]
Active stator odd teeth (1, 3, 5, 7, 9, 11)	0.6
Active stator even teeth (2, 4, 6, 8, 10, 12)	7.4
Profiled stator odd teeth (1, 3, 5, 7, 9, 11)	-0.4
Profiled stator even teeth (2, 4, 6, 8, 10, 12)	4.2

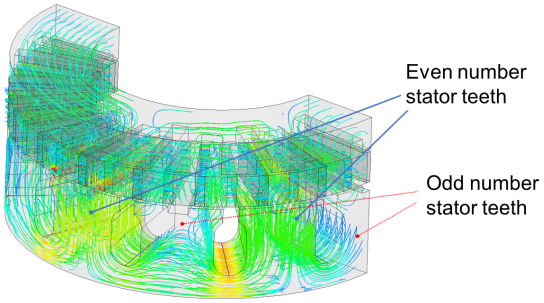

Fig. 3: Magnetic flux for a 3-D FE model. Only half of the machine was modeled to reduce the computational burden. There are in total 990,154 tetrahedral elements. The presented topology has 40 rotor poles and 12 main teeth, each with 2 auxiliary teeth. One of the stators is rotated relative to the other by one rotor pole pitch.

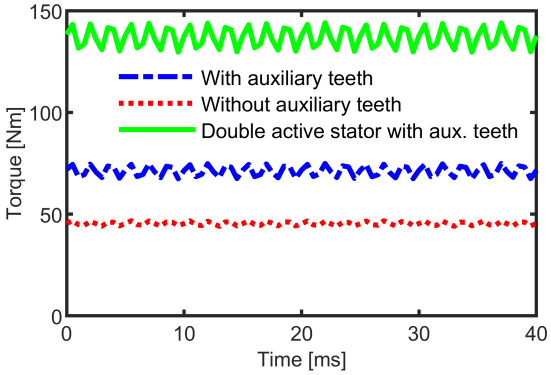

Fig. 4: Torque wave-forms for the 3 topologies shown in Fig. 1. relatively low torque ripple can be observed for the three models.

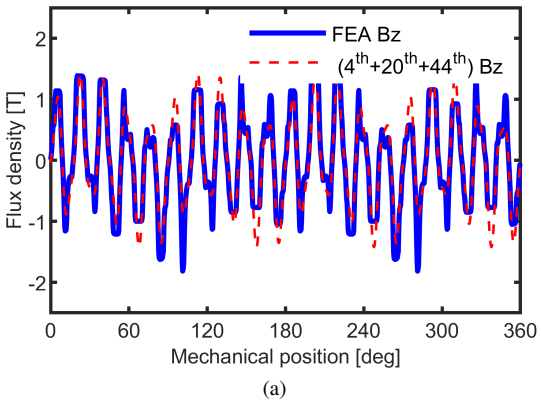

(a)

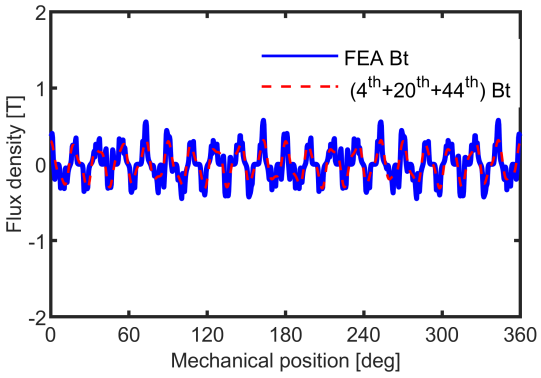

(b)

Fig. 5: Analysis of air-gap flux density distribution in the air-gaps. (a) 3-D FEA predicted axial flux density for the air-gap between active stator and rotor at median diameter, (b) 3-D FEA predicted tangential flux density for the air-gap between active stator and rotor at median diameter

III. Harmonic-based Torque Decomposition

In AFPM machines, the air-gap flux density has two main components, one in the axial- and the other in the tangential-direction. These two components of the air gap flux density distribution at an arbitrary rotor position is obtained from 3-D FEA. The air-gap flux density can be decomposed into a series of harmonics. With the air-gap flux density harmonics, the torque contributed by each harmonic is obtained by:

$$T = r^2 L_{stk} \iint \frac{B_a B_t}{\mu} \mathrm{d}\theta, \tag{3}$$

$$T = \sum_k \left(\frac{D_r}{2}\right)^2 L_{stk} |{B_a}^k||{B_t}^k| \cos({\theta_a}^k - {\theta_t}^k), \tag{4}$$

where D_r is the average diameter of rotor, L_{stk} is the radial stack length of rotor, k is harmonic number, B_a and B_t are the axial and tangential components of flux density in air-gap, respectively.

The axial and tangential components of flux density in the air-gap between the active stator and rotor at the average diameter are extracted from FEA and plotted as shown in Fig. 5(a) and Fig. 5(b). The harmonic spectrum of the axial component waveform, illustrated in Fig. 6(a), shows that only the harmonics of 8, 40, and 88 poles,respectively are substantial and their amplitudes are larger than 0.2T. The reconstructed air-gap flux density waveforms considering the three substantial harmonics are also plotted in Fig. Fig. 5(a) and Fig. 5(b). Torque contributions by 40 pole harmonics are of the largest value in both air-gaps. The 8 pole and 88 pole harmonics can also produces synchronous torque. The torque from the profiled stator side is about half of the active stator side as shown in Fig. 6(b).

IV. Analytical Developments

In this section, the analytical air-gap flux density and corresponding torque equations are deduced. The air-gap PM-MMF under open circuit condition is:

$$F_{PM}(\phi') = F \frac{1}{2h+1} \sin[(2h+1)p_m \phi'], \tag{5}$$

where $(2h+1)p_m$ is the PM pole-pair number.

The air-gap permeance is modeled as a square wave as seen in Fig. 7 and expressed by:

$$\Lambda(\phi) = \frac{\Lambda_{max} + \Lambda_{min}}{2} + \frac{\Lambda_{max} - \Lambda_{min}}{2} \cos[N_{ST}(\phi - \phi_0)] \tag{6}$$

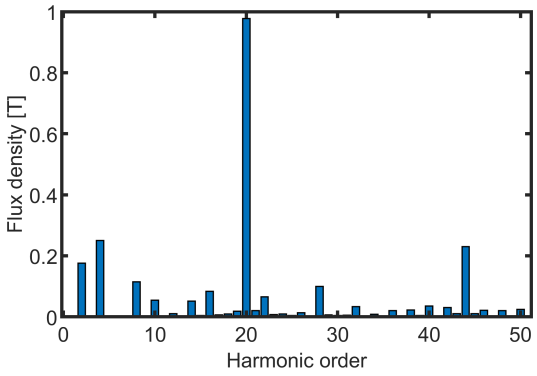

(a)

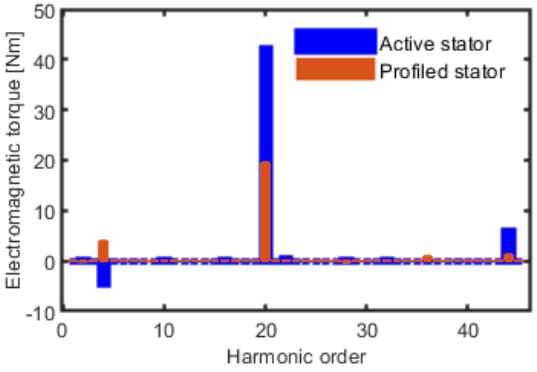

(b)

Fig. 6: Harmonic torque production in the air-gaps. (a) Amplitude spectrum of the axial component of the air-gap flux density and (b) torque contribution of corresponding harmonics for each air-gaps.

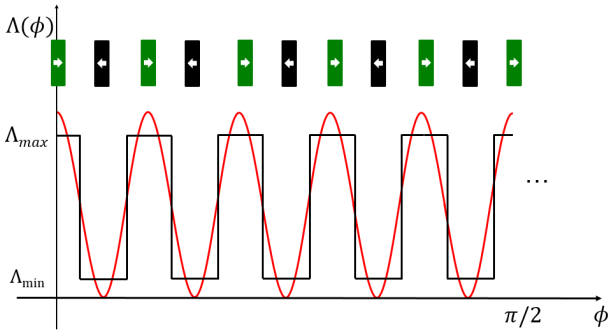

Fig. 7: The air-gap permanence function is modeled as a square-waveform.

where N_{ST} is number of stator teeth.

The angular positions in the rotor and stator reference frames are related to each other by:

$$\phi = \phi' + \theta_r = \phi' + \theta_{r0} + \omega_r t \tag{7}$$

where θ_r is the rotor angle relative to the stator, $\omega_r t$ the rotor speed and θ_{r0} the initial position of rotor with reference to the stator (Fig. 8). The open-circuit air-gap flux density $B_{PM}(\phi)$

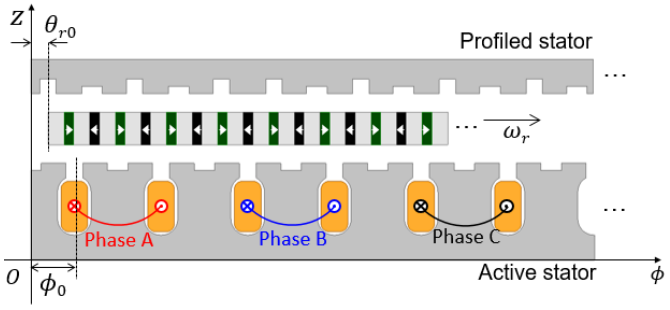

Fig. 8: The coordinate system used for the theoretical analysis. The MAGNUS machine with one active stator and one profiled stator is modeled in 2-D.

can be obtained by multiplying $F_{PM}(\phi)$ and $\Lambda(\phi)$ from (5) and (6):

$$\begin{aligned}
&B_{PM}(\phi) = F_{PM}(\phi) \cdot \Lambda(\phi) = \\
&= F_{PM} \frac{1}{2h+1} \sin[(2h+1)p_m\theta_{r0} + (2h+1)p_m\omega_r t] \cdot \\
&\cdot \left(\frac{\Lambda_{max} + \Lambda_{min}}{2} + \frac{\Lambda_{max} - \Lambda_{min}}{2} \cos[N_{ST}(\phi - \phi_0)] \right) = \\
&= F_{PM} \frac{1}{2h+1} \frac{\Lambda_{max} + \Lambda_{min}}{2} \cdot \\
&\cdot \sin[(2h+1)p_m\theta_{r0} + (2h+1)p_m\omega_r t] + \\
&+ \frac{F_{PM}}{2} \frac{1}{2h+1} \frac{\Lambda_{max} - \Lambda_{min}}{2} \cdot \\
&\cdot \sin[(2h+1)p_m(\theta_{r0} + \omega_r t) + N_{ST}(\phi - \phi_0)] + \\
&+ \frac{F_{PM}}{2} \frac{1}{2h+1} \frac{\Lambda_{max} - \Lambda_{min}}{2} \cdot \\
&\cdot \sin[(2h+1)p_m(\theta_{r0} + \omega_r t) - N_{ST}(\phi - \phi_0)]
\end{aligned} \tag{8}$$

The armature air-gap flux density B_{AR} can be obtained with same approach and employed for the derivation of electromagnetic torque analysis T_{em} as follow:

$$\begin{aligned}
&T_{em} = \frac{\partial W_{co}}{\partial \theta_r} = \frac{\partial}{\partial \theta_r} \int_V \frac{B(\phi,t)^2}{2\mu} \, dv = \\
&= \frac{D_r g L_{stk}}{4\mu} \frac{\partial}{\partial \theta_r} \int_0^{2\pi} (B_{PM}(\phi,t) + B_{AR}(\phi,t))^2 \, d\phi,
\end{aligned} \tag{9}$$

where D_r is the average diameter, g is air-gap, and L_{stk} is radial stack length.

V. Prototyping

Prototyping of the proposed MAGNUS AFPM motor is underway. The stator and rotor cores were fabricated using

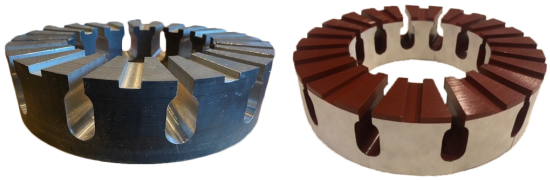

Fig. 9: Active stator core machined from a laminated steel ring, before surface treatment.

Fig. 10: The prototyped profiled stator core and active stator wound with coils.

laminated M15_29G steel rings to provide optimal performance. The machined active stator core and the surface trated version can be seen in Fig. 9. Each tooth is wounded with coils in the active stator providing opportunities to perform experimental studies with different winding configuration. The active stator with coils and profiled stator are shown in Fig. 10. The 40-pole rotor is currently being manufactured.

Experimentation is planned using the proposed test fixture from Fig. 11. The test procedure can be conducted with different air-gap length by adjusting the distance between the adapter plate and the cylindrical spacer.

VI. Conclusion

The torque production for a novel vernier-type AFPM machine topology named MAGNUS has been analyzed through two methods based on the Maxwell stress on individual stator and rotor components and on the harmonic analysis of the air-gap flux density, respectively. The machine has one 3-phase stator wound with 6 coils only, one profiled stator without coils, and a 40-pole spoke-type PM rotor. It has been shown that the torque contributed by the wound active stator is almost twice that of the profiled stator. It was also shown that half of the main stator teeth produce the majority of the torque. The effect of the auxiliary teeth on increasing the torque output by approx. 61% has also been identified. The manufacturing of a prototype motor with double layer concentrated winding and a special spoke rotor with slot bridges is underway to allow testing of design variations.

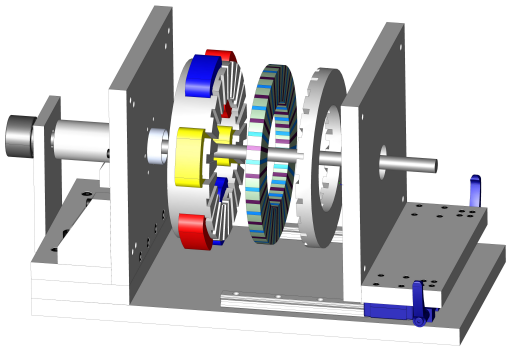

Fig. 11: Designed machine test fixture for experimental setup.

Acknowledgment

This material is based upon work supported by the National Science Foundation (NSF) under Grant No. 1809876. Any opinions, findings, and conclusions or recommendations expressed in this material are those of the authors and do not necessarily reflect the views of the NSF. The support of University of Kentucky, the L. Stanley Pigman Endowment, and of ANSYS, Inc. is also gratefully acknowledged.

References

[1] D. M. Ionel, J. F. Eastham, and T. Betzer, "Finite element analysis of a novel brushless dc motor with flux barriers," *IEEE Transactions on Magnetics*, vol. 31, no. 6, pp. 3749–3751, 1995.

[2] A. Fatemi, D. M. Ionel, M. Popescu, Y. C. Chong, and N. A. O. Demerdash, "Design optimization of a high torque density spoke-type pm motor for a formula e race drive cycle," *IEEE Transactions on Industry Applications*, vol. 54, no. 5, pp. 4343–4354, 2018.

[3] P. M. Tlali, R. Wang, and S. Gerber, "Comparison of PM vernier and conventional synchronous 15 kW wind generators," in *Proc. Int. Conf. Electr. Mach. (ICEM)*, Sep. 2018, pp. 2065–2071.

[4] V. Rallabandi, N. Taran, D. M. Ionel, and I. G. Boldea, "MAGNUS — an ultra-high specific torque PM axial flux type motor with flux focusing and modulation," in *2017 IEEE Energy Conversion Congress and Exposition (ECCE)*, 2017, pp. 1234–1239.

[5] R. Zhang, J. Li, R. Qu, and D. Li, "Analysis and design of triple-rotor axial-flux spoke-array vernier permanent magnet machines," *IEEE Transactions on Industry Applications*, vol. 54, no. 1, pp. 244–253, 2018.

[6] V. Rallabandi, P. Han, M. G. Kesgin, N. Taran, and D. M. Ionel, "Axial-field vernier-type flux modulation machines for low-speed direct-drive applications," in *Proc. IEEE Energy Convers. Congr. Expo. (ECCE)*, Sep. 2019, pp. 3123–3128.

[7] M. G. Kesgin, P. Han, N. Taran, and D. M. Ionel, "Optimal study of a high specific torque vernier-type axial-flux PM machine with two different stators and a single winding," in *2020 IEEE Energy Conversion Congress and Exposition (ECCE)*, 2020, pp. 4064–4067.

[8] S. Choi, M. S. Haque, M. T. B. Tarek, V. Mulpuri, Y. Duan, S. Das, V. Garg, D. M. Ionel, M. A. Masrur, B. Mirafzal, and H. A. Toliyat, "Fault diagnosis techniques for permanent magnet ac machine and drives—a review of current state of the art," *IEEE Transactions on Transportation Electrification*, vol. 4, no. 2, pp. 444–463, 2018.

[9] Y. Oner, Z. Q. Zhu, L. J. Wu, X. Ge, H. Zhan, and J. T. Chen, "Analytical on-load subdomain field model of permanent-magnet vernier machines," *IEEE Transactions on Industrial Electronics*, vol. 63, no. 7, pp. 4105–4117, 2016.

[10] F. Zhao, T. A. Lipo, and B. Kwon, "A novel dual-stator axial-flux spoke-type permanent magnet vernier machine for direct-drive applications," *IEEE Transactions on Magnetics*, vol. 50, no. 11, pp. 1–4, 2014.

[11] Z. Z. Wu and Z. Q. Zhu, "Analysis of air-gap field modulation and magnetic gearing effects in switched flux permanent magnet machines," *IEEE Transactions on Magnetics*, vol. 51, no. 5, pp. 1–12, 2015.